These findings contrast with the role typically assigned to osteopontin in most mineralization models, where it often acts as an inhibitor of crystal growth and/or nucleation (Steitz et al. 2002; Johnson et al. 2003). Our work involves a different crystal type, and ample evidence suggests that factors that clearly inhibit calcium phosphate crystal formation may stimulate CPPD crystal formation. Inorganic pyrophosphate is perhaps the best characterized example of such a factor. Pyrophosphate inhibits hydroxyapatite crystal nucleation and growth, yet is absolutely required for CPPD crystal formation. Many of the studies demonstrating direct inhibitory effects of osteopontin on calcium crystal formation used fairly high osteopontin concentrations (Gericke et al. 2005), or systems in which the osteopontin remains soluble and is not incorporated into matrix (Beshensky et al. 2000). In contrast, a small number of previous studies showed that in small concentrations or with low phosphorylation states, osteopontin may stimulate calcium phosphate mineral formation (Jono et al. 2000). Taken together, these studies suggest that osteopontin has multiple and complex effects on mineralization.

A great deal of work focuses on the phosphorylation state of osteopontin in mineralization models. Tissue osteopontin is generally not as highly phosphorylated as milk osteopontin, but it is highly unlikely that completely de-phosphorylated osteopontin would be encountered by chondrocytes. We showed that highly phosphorylated forms of osteopontin were slightly more potent stimulants of CPPD crystal formation compared to less phosphorylated forms. In many mineralization models, de-phosphorylated osteopontin had opposite effects to those seen with highly phosphorylated osteopontin (Jono et al. 2000). This is not true of osteopontin in our model. Thus, it is unlikely that the effect of osteopontin in our system is highly dependent on its anionic charge or that it acts by simply coating existing crystals and altering their growth.

Osteopontin is clearly a transglutaminase substrate in articular cartilage and cultured chondrocytes. We proved this by demonstrating that transglutaminase inhibitors decrease its levels in chondrocyte matrix, that specific transglutaminase crosslinks are easily measurable in isolated cartilage osteopontin, and that active transglutaminases reside in the pericellular matrix of CPPD affected chondrocytes in a distribution similar to that of osteopontin. Transglutaminase-mediated incorporation of osteopontin into matrix augments the effect of osteopontin on CPPD crystal formation. Indeed, when transglutaminase activity is suppressed, osteopontin fails to stimulate CPPD crystal deposition. We postulate that the high levels of active transglutaminases in osteoarthritic cartilage trap osteopontin in the extracellular matrix, where it stimulates mineralization. The dose response curve for both milk and recombinant osteopontin demonstrates a bell shaped curve, with a maximum effect occurring at about 1 μg/ml. We hypothesize that chondrocyte matrix can only incorporate a certain quantity of osteopontin. At doses which exceed the capacity of the matrix to incorporate osteopontin, osteopontin remains soluble and may actually begin to inhibit CPPD crystal growth.

One could postulate several mechanisms through which osteopontin might contribute to CPPD crystal formation. Osteopontin might stimulate production of pyrophosphate, the anionic component of the CPPD crystals. We show here, however, that osteopontin has minimal effects on pyrophosphate production by chondrocytes. It is also possible that osteopontin modulates cell death, which then leads to CPPD crystal formation (Jaovisidha et al. 2002). However, osteopontin had no effect on the viability of chondrocytes at the doses employed in these studies. We also investigated the possibility that osteopontin stimulates transglutaminase activity. Surprisingly, osteopontin stimulated transglutaminase activity in chondrocytes in a dose-responsive manner. Protein levels of the chondrocyte transglutaminases, factor XIIIA and type II transglutaminase, were unaffected by osteopontin. Thus, it is likely that osteopontin activates existing transglutaminase enzymes rather than increasing their protein levels. Both type II transglutaminase and factor XIIIA are often post-translationally regulated. For example, thrombin and other serine proteases activate factor XIIIA, and type II transglutaminase activity is tightly regulated by ambient levels of calcium and GTP.

Mirroring work done in osteoblasts, we showed that the effect of osteopontin on CPPD crystal formation was partially abrogated by a peptide which blocks integrin binding. Thus, we propose that crosslinked complexes containing osteopontin acting via the αvβ3 integrin serve as foci of CPPD crystal nucleation. This is further supported by the effect of thrombin on osteopontin, as the thrombin cleavage site is near the integrin binding locus of the protein. It is likely that chondrocytes are capable of assuming a phenotype similar to the hypertrophic phenotype responsible for bone formation in the growth plate, particularly in the setting of osteoarthritis (Kirsch et al. 2000). Thus, it is not surprising that mechanisms of matrix mineralization in articular chondrocytes are similar to that of bone cells under certain conditions.

These studies are not without limitations. For example, there is not a simple way to determine if the effects of osteopontin are mediated by the protein itself, or by osteopontin-induced increases in transglutaminase activity, and a consequent increase in the quantity of cross-linked matrix. In either event, however, the actions of osteopontin clearly stimulate CPPD crystal formation, and this protein may represent a therapeutic target in this disease. In addition, non-specific effects of chemical transglutaminase inhibitors are always a concern. Monodansylcadaverine, for example, did reduce protein levels of both aggrecan and osteopontin secreted into the media. However, its effects on osteopontin levels in the matrix were quite specific, and aggrecan levels were unaffected. We have considerable experience with these inhibitors and approach their limitations by using at least two inhibitors with different mechanisms of action, by ensuring the absence of toxicity, and by comparing their effects under various conditions such as the presence and absence of ATP. Unfortunately, because there are at least two active transglutaminase enzymes in articular cartilage, the use of more specific inhibitors such as antibodies or siRNA becomes too unwieldy to be practical.

We have shown here that osteopontin promotes CPPD crystal formation in a well characterized, chondrocyte-based model. Osteopontin is present in articular cartilage affected by CPPD deposition and may be an important factor in the development of CPPD crystals *in vivo*. Ultimately, identifying participants involved in CPPD crystal formation may lead to the development of new interventions for CPPD crystal formation and the ensuing cartilage degeneration.

Acknowledgements

We would like to acknowledge the thoughtful assistance of Drs. Lawrence M. Ryan and Jeffrey Wesson in reviewing this manuscript. This work was supported by the National Institutes of Health AG015337 (AKR), and AR 052615 (AKR) and the Veteran's Administration Research Service (AKR).

REFERENCES

Beninati S, Senger D, Cordella-Miele E, Mukherjee A, Chackalaparampil I, Shanmugam V, Singh K, Mukherjee B. Osteopontin:Its transglutaminase-catalyzed posttranslational modifications and cross-linking to fibronectin. J Biochem 1994;115:675–82. [PubMed: 7916341]

Beshensky A, Wesson J, Kleinman J, Liaw L, Steitz S, Giachelli C, et al. Renoprotective modulation of calcium oxalate studcture by osteopontin in vivo. J Am Soc Nephrol 2000;11:558A.

Beshensky A, Wesson J, Worcester E, Sorokina E, Snyder C, Kleinman J. Effects of urinary macomolecules on hydroxyapatite crystal formation. J Am Soc Nephrol 2001;12:2108–16. [PubMed: 11562409]

Beutler A, Rothfuss S, Clayburne G, Sieck M, Schmacher H Jr. Calcium pyrophosphate dihydrate crystal deposition in synovium. Arthritis Rheum 1993;36:704–15. [PubMed: 8489549]

Bjelle A. Cartilage matrix in hereditary pyrophosphate arthropathy. J Rheumatol 1981;8:959–964. [PubMed: 6276539]

Cheung H. Calcium crystal effects on the cells of the joint: implications for the pathogenesis of disease. Curr Opinion Rheumatology 2001;12:223–7.

Denhardt D, Noda M, O'Regan A, Pavlin D, Berman J. Osteopontin as a means to cope with environmental insults:regulation of inflammation, tissue remodeling, and cell survival. J Clin Invest 2001;107:1055–61. [PubMed: 11342566]

Derfus B, Kurian J, Butler J, Daft L, Carrera G, Ryan L, Rosenthal A. The high prevalence of pathologic calcium crystals in pre-operative knees. J Rheumatol 2002;29:570–4. [PubMed: 11908575]

Gericke A, Qin C, Spevak L, Fujimoto Y, Bultler W, Sorensen E, Boskey A. Importance of phosphorylation for osteopontin regulation of biomineralization. Calcif Tissue Int 2005;77:45–54. [PubMed: 16007483]

Giachelli C, Speer M, Li X, Rajachar R, Yang H. Regulation of vascular calcification: roles of phosphate and osteopontin. Circ Res 2005;96:717–22. [PubMed: 15831823]

Goldberg H, Hunter G. The inhibitory activity of osteopontin on hydroxyapatite formation in vitro. Ann NY Acad Sci 1995;760:305–8. [PubMed: 7785906]

Harmey D, Hessle L, Narisawa S, Johnson K, Terkeltaub R, Millan J. Concerted regulation of inorganic pyrophosphate and osteopontin by *Akp2, Enpp1* and *Ank*. Am J Pathol 2004;164:1199–1209. [PubMed: 15039209]

Heinkel D, Gohr C, Uzuki M, Rosenthal A. Transglutaminase contributes to CPPD crystal formation in osteoarthritis. Frontiers in Bioscience 2004;9:3257–61. [PubMed: 15353354]

Ishikawa K, Masuda I, Ohira T, Yokoyama M. A histologic study of calcium pyrophosphate dihydrate crystal-deposition disease. J Bone Jt Surg 1989;71:875–86.

Jaovisidha K, Rosenthal A. Calcium crystals in osteoarthritis. Curr Opin Rheumatol 2002;14:298–302. [PubMed: 11981330]

Johnson K, Goding J, Van Etten D, Sali A, Hu S-I, Farley D, Krug H, Hessle L, Millan J, Terkeltaub R. Linked deficiencies in extracellular PPi and osteopontin mediate pathologic calcification associated with defective PC-1 and ANK expression. J Bone Miner Res 2003;18:994–1002. [PubMed: 12817751]

Johnson K, Hashimoto S, Lotz M, Pritzker K, Terkeltaub R. Interleukin-1 induces pro-mineralizing activity of cartilage tissue transglutaminase and factor XIIIa. Am J Pathol 2001;159:149–63. [PubMed: 11438463]

Johnson K, van Etten D, Nanda H, Grahm R, Terkeltaub R. Distinct transglutaminase 2-independent and transglutaminase 2-dependent pathways mediate articular chondrocyte hypertrophy. J Biol Chem 2003;278:18824–32. [PubMed: 12606540]

Jono S, Giachelli C. Phosphorylation of osteopontin is required for inhibition of vascular smooth muscle cell calcification. J Biol Chem 2000;275:20197–203. [PubMed: 10766759]

Kaartinen M, Pirhonen A, Linnala-Kankkunen A, Maenpaa P. Cross-linking of osteopontin by tissue transglutaminase increases its collagen binding properties. J Biol Chem 1999;274:1729–35. [PubMed: 9880554]

Kirsch R, Swoboda B, Nah H-D. Activation of annexin II and V expression, terminal differentiation, mineralization and apoptosis in human osteoarthritic cartilage. Osteoarthritis Cartilage 2000;8:294–302. [PubMed: 10903884]

Ledingham J, Regan M, Jones A, Doherty M. Radiographic patterns and associations of osteoarthritis of the knee in patients referred to hospital. Ann Rheum Dis 1993;52:520–6. [PubMed: 8346979]

Lorand L, Graham R. Transglutaminases: crosslinking enzymes with pleiotrophic functions. Nature 2003;4:140–57.

Mandel N, Mandel G, Carroll D, Halverson P. Calcium pyrophosphate crystal deposition: An in vitro study using a gelatin matrix model. Arthritis Rheum 1984;27:789–96. [PubMed: 6331461]

Masuda I, Ishikawa K, Usuku G. A histologic and immunohistochemical study of calcium pyrophosphate dihydrate crystal deposition disease. Clin Orth 1991;263:272–287.

McCarty D, Hogan J, Gatter R, Grossman M. Studies on pathological calcifications in human cartilage I. Prevalence and types of crystal deposits in the menisci of two hundred fifteen cadavers. J Bone Jt Surg 1966;48A:309–25.

McCarty, DJ. Pseudogout: articular chondrocalcinosis; calcium pyrophosphate crystal deposition disease. In: Hollander, J.; McCarty, D., Jr., editors. Arthritis and Allied Conditions. Eighth Edition. Lea & Febiger; Philadelphia: 1972. p. 1140-60.

Mitchell P, Struve J, McCarthy G, Cheung H. Basic calcium phosphate crystals stimulate cell proliferation and collagenase message accumulation in cultured adult articular chondrocytes. Arthritis Rheum 1992;35:343–350. [PubMed: 1311178]

Nalbant S, Martinez J, Kitumnuaypong T, Clayburne G, Sieck M, Schumacher H Jr. Synovial fluid features and their relations to osteoarthritis severity: new findings from sequential studies. Osteoarthritis Cart 2003;11:50–4.

Parikh A, Lee G, Tchivilev I, Graff R. A neocartilage ideal for extracellular matrix macromolecule immunolocalization. Histochem Cell Biol 2003;120:427–34. [PubMed: 14593482]

Pullig O, Weseloh G, Gauer S, Swoboda B. Osteopontin is expressed by adult human osteoarthritic chondrocytes: protein and mRNA analysis of normal and osteoarthritic cartilage. Matrix Biology 2000;19:245–55. [PubMed: 10936449]

Rosenthal A, Cheung H, Ryan L. Transforming growth factor beta 1 stimulates inorganic pyrophosphate elaboration by porcine cartilage. Arthritis Rheum 1991;34:904–911. [PubMed: 1647773]

Rosenthal A, Mosesson M, Gohr C, Masuda I, Heinkel D, Siebenlist K. Regulation of transglutaminase activity in articular chondrocytes through thrombin receptor-mediated factor XIII synthesis. Thromb Haemost 2004;91:558–68. [PubMed: 14983233]

Rosenthal AK, Derfus BA, Henry LA. Transglutaminase activity in aging articular chondrocytes and articular cartilage vesicles. Arthritis Rheum 1997;40(5):966–970. [PubMed: 9153560]

Ryan L, Kurup I, Derfus B, Kushnaryov V. ATP-induced chondrocalcinosis. Arthritis Rheum 1992;35:1520–4. [PubMed: 1472129]

Ryan L, Rosenthal A. Metabolism of extracellular pyrophosphate. Curr Opin Rheum 2003;15:311–4.

Steitz S, Speer M, McKee M, Liaw L, Almeida M, Yang H, Giachelli C. Osteopontin inhibits mineral deposition and promotes regression of ectopic calcification. Am J Pathol 2002;161:2035–46. [PubMed: 12466120]

Summey BJ, Graff R, Lai T, Greenberg C, Lee G. Tissue transglutaminase localization and activity regulation in the extracellular matrix of articular cartilage. J Orth Res 2002;20:76–82.

Wozniak M, Fausto A, Carron C, Meyer D, Hruska K. Mechanically strained cells of the osteoblast lineage organize their extracellular matrix through unique sites of αv β3-integrin expression. J Bone Min Res 2000;15:1731–40.

Yamamoto N, Sakai F, Kon S, Morimoto J, Kimura C, Yamazaki H, Okazaki I, Seki N, Fujii T, Uede T. Essential role of the cryptic epitope SLAYGLR within osteopontin in a murine model of rheumatoid arthritis. J Clin Invest 2003;112:181–8. [PubMed: 12865407]

Yokosaki Y, Tanaka K, Higashikawa F, Yamashita K, Eboshida A. Distinct structural requirements for binding of the integrins alphavbeta6, alphavbeta3, alphavbeta5, alphavbeta1 and alpha9beta1 to osteopontin. Matrix Biol 2005;24:418–27. [PubMed: 16005200]

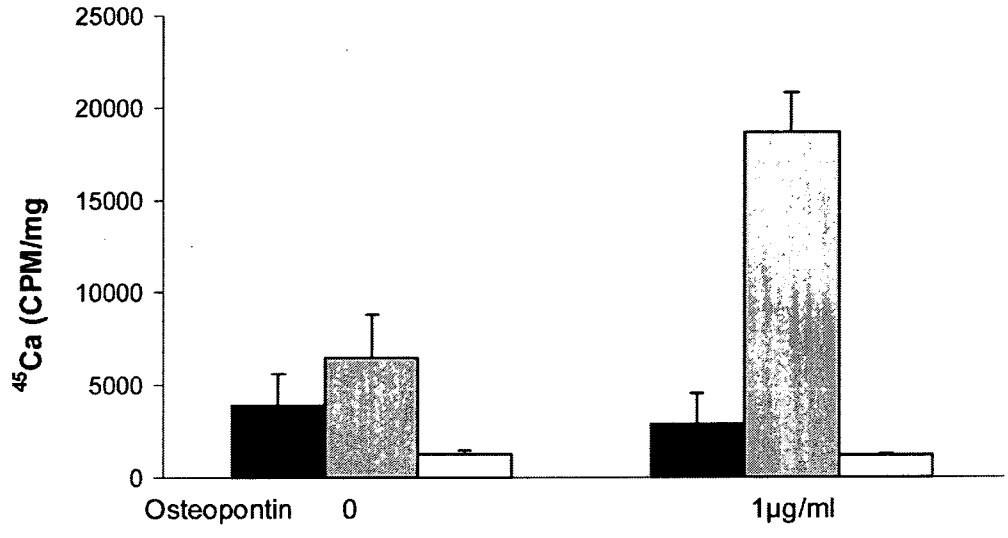

Figure 1.

The effect of recombinant osteopontin in a model of CPPD crystal formation in chondrocytes. Chondrocytes were incubated with 1 µg/ml recombinant osteopontin and ^{45}Ca, with or without 1 mM ATP or 1 mM β glycerophosphate. After 48 hours, media were removed and cell layers were washed. ^{45}Ca levels in the cell layer were measured with liquid scintigraphy and corrected for cell protein. Black bars represent results with no ATP. Grey bars represent results with ATP. White bars represent results with β-glycerophosphate. Values are means ± standard errors (n=25). Osteopontin significantly increased ^{45}Ca precipitation in the presence of ATP, reflecting increased CPPD crystal formation ($p<0.01$).

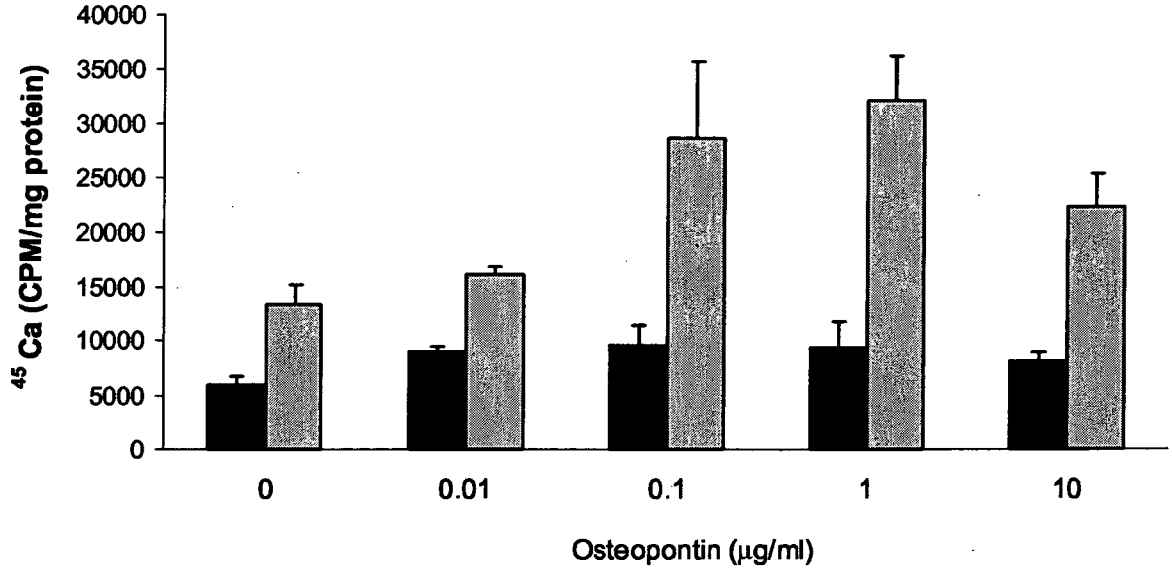

Figure 2.

The effect of various doses of recombinant osteopontin on CPPD crystal formation. Chondrocytes were incubated with varying doses of recombinant osteopontin in the presence of ^{45}Ca with or without 1 mM ATP. After 48 hours, media were removed, and cell layers were thoroughly washed. ^{45}Ca levels in the cell layer were measured with liquid scintigraphy and corrected for cell protein. Black bars represent results with no ATP. Grey bars represent results with ATP. Values are means ± standard deviations (n=6). Concentrations of osteopontin less than 0.1 μg/ml or greater than 10 μg/ml did not statistically significantly increase CPPD crystal formation.

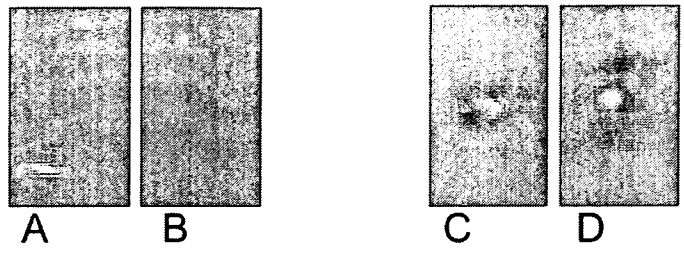

Figure 3.
Polarizing light microscopy of crystals generated by chondrocyte monolayers. Chondrocytes were incubated with 1 mM ATP with or without recombinant osteopontin for 48 hours. The cell layers were scraped onto slides and viewed under polarizing light microscopy. CPPD crystals appear as rhomboidal positively birefringent structures. Crystals were yellow when perpendicular to the axis of the polarizer and blue when parallel. The same field was photographed in two orientations at 90 degree angles to one another. A) and B) are cell layers incubated with ATP; C) and D) are cell layers incubated with osteopontin and ATP.

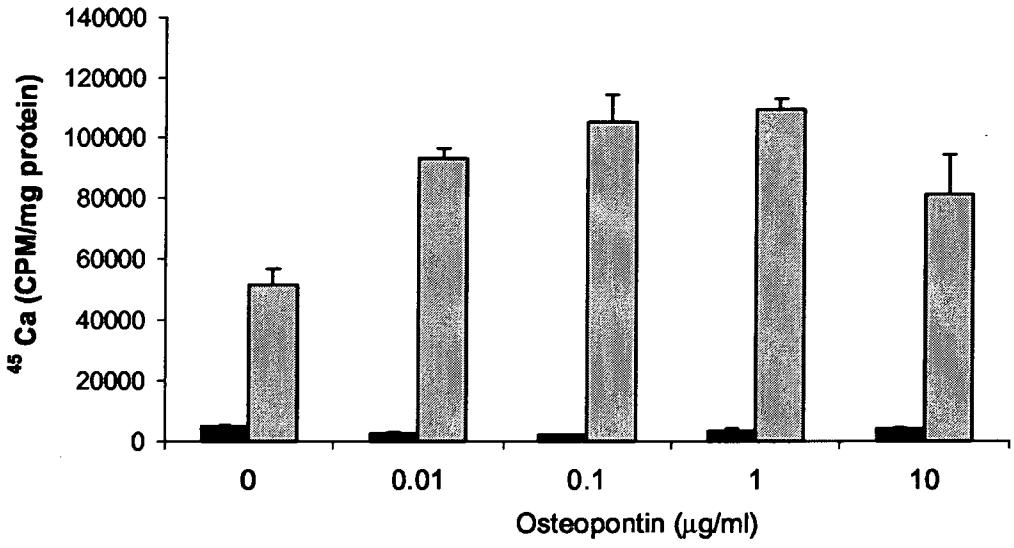

Figure 4.

The effect of various doses of milk osteopontin on CPPD crystal formation. Chondrocytes were incubated with varying doses of milk osteopontin in the presence of ^{45}Ca with or without 1 mM ATP. After 48 hours, media were removed, and cell layers were thoroughly washed. ^{45}Ca levels in the cell layer were measured with liquid scintigraphy and corrected for cell protein. Black bars represent results with no ATP. Grey bars represent results with ATP. Values are means ± standard deviations (n=6).

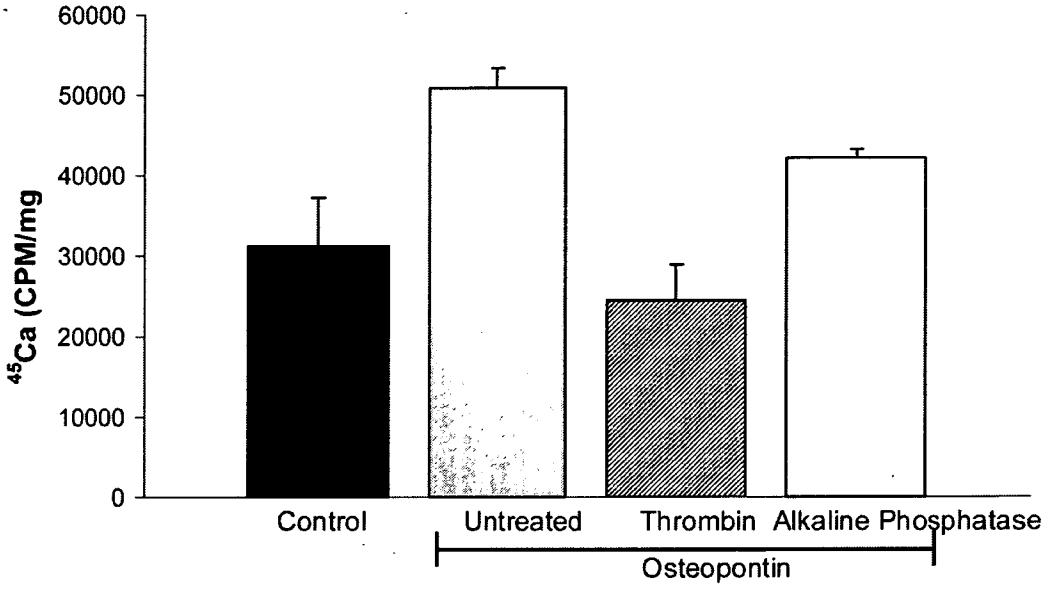

Figure 5.

The effect of de-phosphorylation and thrombin-cleavage on osteopontin's ability to stimulate CPPD crystal formation. Chondrocytes were incubated with no additives (Control, black bar), 1 μg/ml untreated milk osteopontin (grey bar), 1 μg/ml thrombin-cleaved osteopontin (hatched bar), or 1 μg/ml alkaline-phosphatase treated osteopontin (white bar) in the presence of ^{45}Ca and 1 mM ATP. After 48 hours, media were removed, and the cell layers were washed. ^{45}Ca levels were determined in the cell layer and corrected for cell protein. Results are expressed as means ± standard deviations (n=4). Thrombin-treated osteopontin is no different from control ($p=0.25$). Alkaline phosphatase treatment of osteopontin reduced its effects ($p<.003$), but levels of CPPD crystal formation remained significantly higher than control values ($p<.05$).

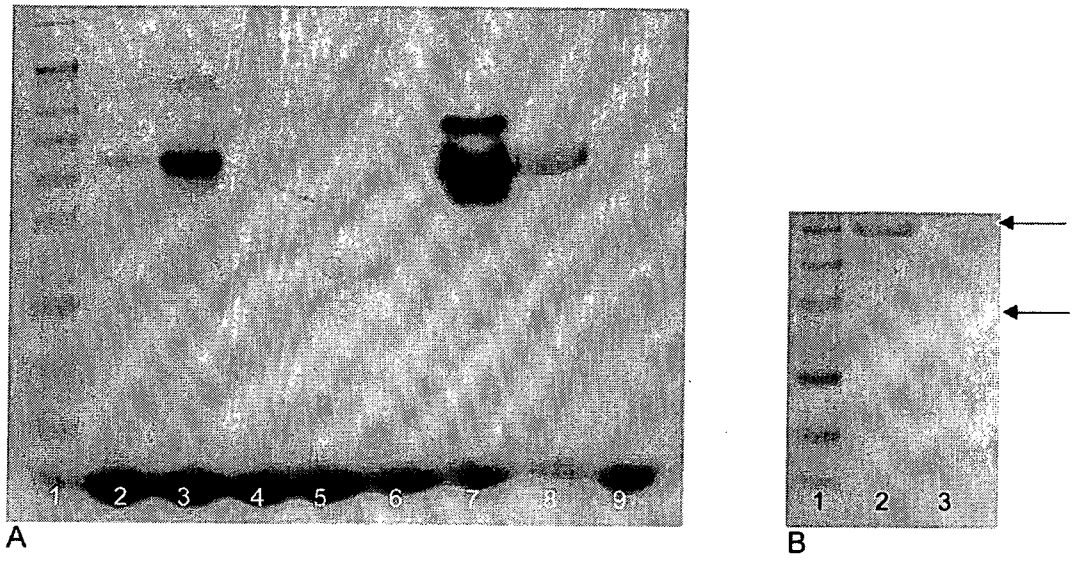

Figure 6.

Staining for phosphorylation of osteopontin and quantitative cleavage of osteopontin by thrombin. A) Identical quantities of various preparations of osteopontin were stained for phosphorylation using GelCode phosphoprotein stain according to the manufacturer's directions. Lane1: molecular weight markers , Lane 2: 1 μg positive control, Lane 3: 10 μg positive control, Lane 4: 1 μg negative control, Lane 5: 10 μg negative control, Lane 6: 10 μg recombinant osteopontin, Lane 7: 10 μg milk osteopontin, Lane 8: 10 μg human osteopontin (Assay Designs), Lane 9: 10 μg alkaline phosphatase-treated milk osteopontin.

B) SDS Page of osteopontin before and after cleavage by thrombin. Milk osteopontin was exposed to thrombin coated beads and samples were run on an SDS PAGE gel before and after thrombin exposure. There is quantitative cleavage of osteopontin by thrombin. Lane 1: molecular weight marker, Lane 2: untreated osteopontin, Lane 3: thrombin treated osteopontin

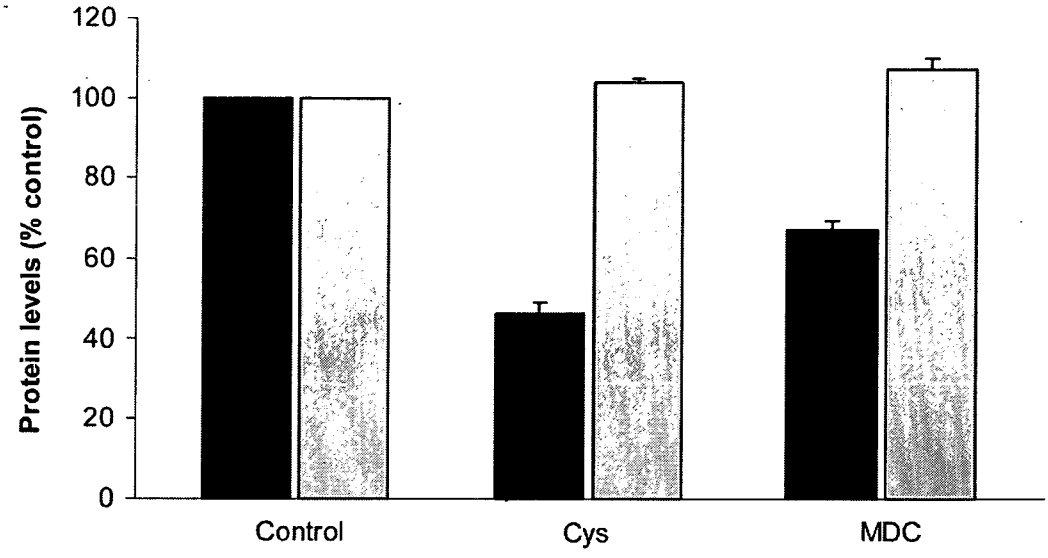

Figure 7.

The effect of transglutaminase inhibitors on levels of osteopontin and aggrecan in chondrocyte cell layers. Chondrocytes were incubated with or without the transglutaminase inhibitors cystamine (Cys, 125μM) or monodansylcadaverine (MDC, 1 mM) for 24 hours. Levels of osteopontin and aggrecan were determined in the cell layer with ELISAs and corrected for protein levels in the samples. Results are normalized to the control (no inhibitor), and expressed as means ± standard deviations (n =6). The transglutaminase inhibitors reduced osteopontin levels (black bars, $p<0.05$), but had no effects on levels of aggrecan (grey bars). Levels of these proteins in the media were unchanged with cystamine, and moderately decreased by monodansylcadaverine.

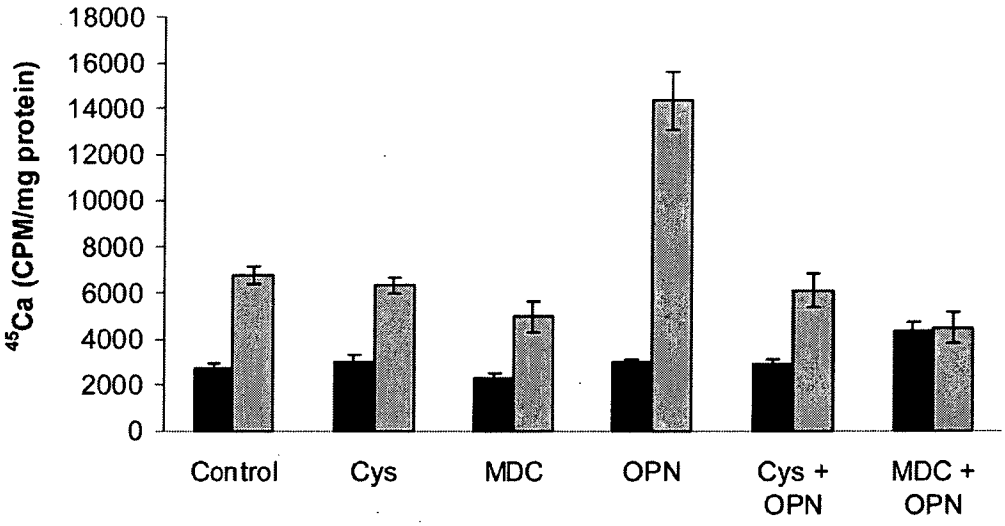

Figure 8.

The effect of transglutaminase inhibitors on osteopontin's ability to stimulate CPPD crystal formation. Chondrocytes were incubated with 1 μg/ml milk osteopontin (OPN) in media containing ^{45}Ca with or without 1 mM ATP. Some chondrocyte cultures were exposed to the transglutaminase inhibitors cystamine (Cys, 125μM) or monodansylcadaverine (MDC, 1 mM). After 48 hours, media were removed, cell layers were washed, and ^{45}Ca levels in the cell layer were quantified with liquid scintigraphy and corrected for cell protein. Black bars represent results with no ATP. Grey bars represent results with ATP. Values represent means ± standard deviations (n=16). Both cystamine and monodansylcadaverine significantly reduced the effects of osteopontin on CPPD crystal formation ($p<0.001$).

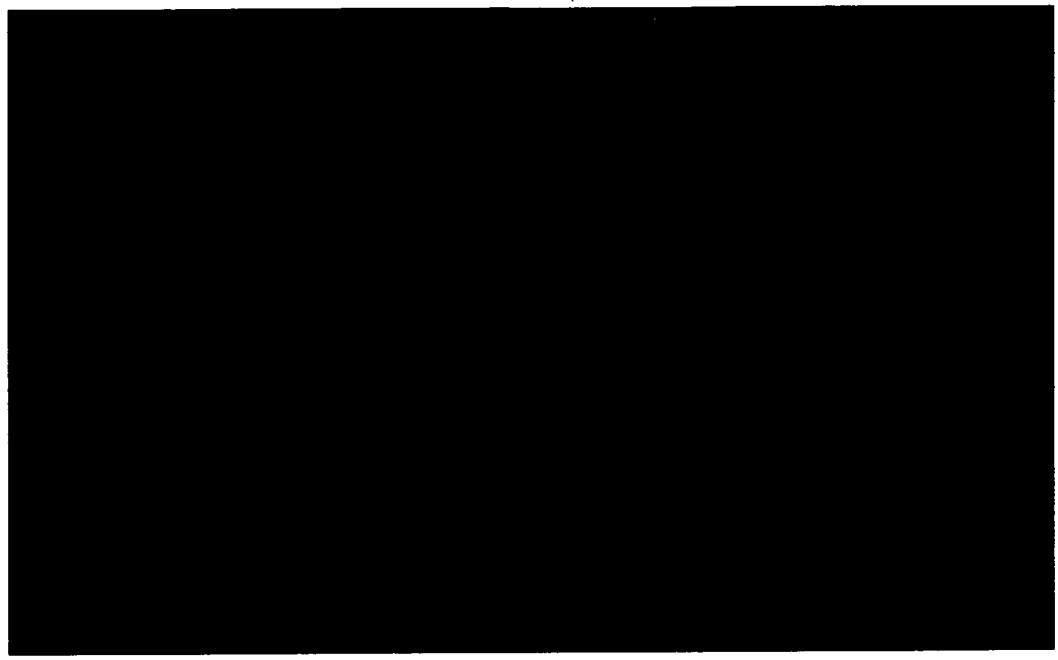

Figure 9.
The effect of osteopontin on chondrocyte transglutaminase activity. Chondrocytes were incubated with various doses of milk osteopontin for 48 hours. Transglutaminase activity was measured in the cell layer using a standard radiometric assay, and was corrected for protein in the sample. Osteopontin significantly increased transglutaminase activity at all concentrations tested ($n= 4$, $p < 0.01$).

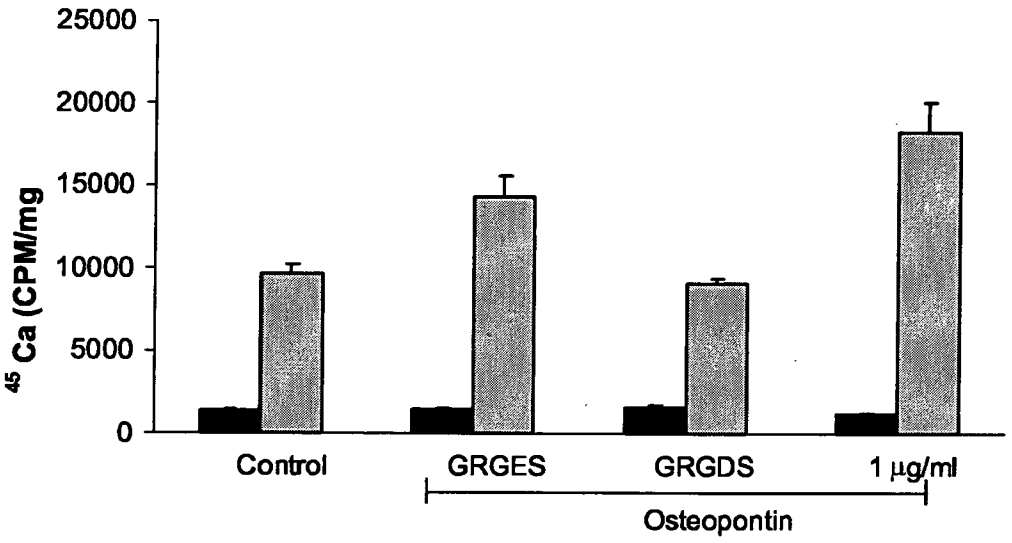

Figure 10.

The effect of an integrin antagonist on osteopontin-induced stimulation of CPPD crystal formation. Chondrocytes were incubated with no additives (Control), 40 µM inactive peptide control (GRGES), 40 µM integrin antagonist (GRGDS) or 1 µg/ml milk osteopontin in the presence of ^{45}Ca and with or without 1 mM ATP. After 48 hours, media were removed, and cell layers were thoroughly washed. ^{45}Ca levels in the cell layer were measured with liquid scintigraphy and corrected for cell protein. Black bars represent results with no ATP. Grey bars represent results with ATP. Values are means ± standard deviations (n=12). Over multiple experiments, the GRGES peptide had no statistically significant effect on osteopontin-induced CPPD crystal formation at doses of 5-40 µM (p=.06), while the GRGDS peptide significantly reduced osteopontin-induced CPPD crystal formation ($p \leq .001$)

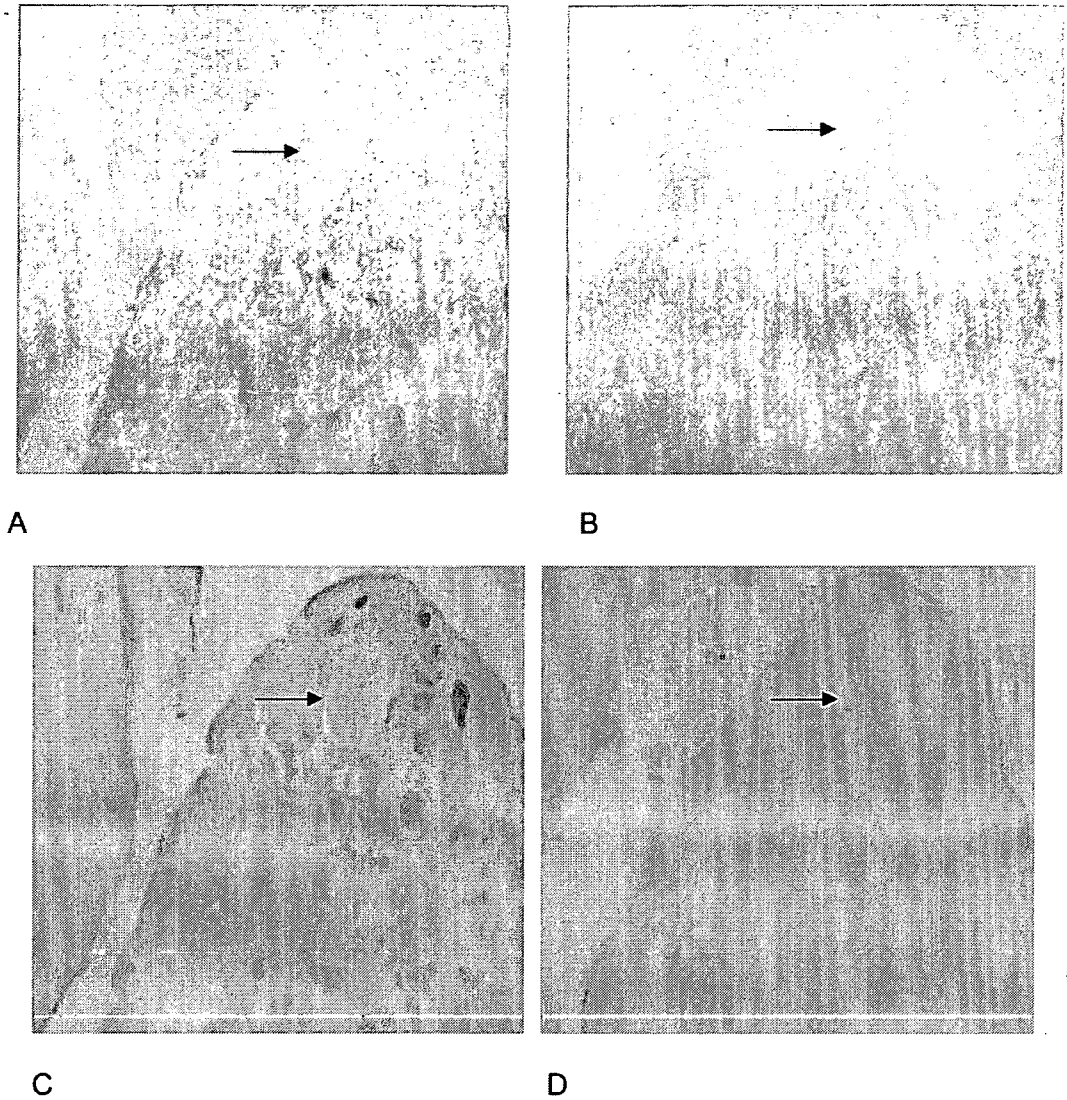

Figure 11.
Distribution of osteopontin and transglutaminase crosslinks in human CPPD-diseased articular cartilage. Immunohistochemistry was performed with anti-osteopontin antibody (Panel A), non-immune rabbit serum (Panel B), or antibody to the transglutaminase specific crosslink (Panel C), or non-immune mouse serum (Panel D) in human CPPD diseased articular cartilage. Arrows demonstrate CPPD crystals in the tissue slices. The presence of immunoreactive protein is demonstrated by brown staining.

TABLE 1

The effect of osteopontin on pyrophosphate levels in chondrocyte cultures.

Osteopontin (μg/ml)	Pyrophosphate (μM)**
0	2.6± 0.2
0.1	3.1± 0.6
1	3.3± 0.7
10	2.3± 0.1
25	2.3± 0.01

** Various concentrations of milk osteopontin were added to chondrocyte cultures. After 48 hours, pyrophosphate levels were measured in conditioned media. Values represent means ± standard deviations (n=6). Osteopontin did not significantly affect pyrophosphate levels at any concentration (p= 0.1).

ELSEVIER

Bone 40 (2007) 876–887

BONE

www.elsevier.com/locate/bone

Effects of aromatase inhibitors on human osteoblast and osteoblast-like cells: A possible androgenic bone protective effects induced by exemestane

Yasuhiro Miki [a], Takashi Suzuki [a], Masahito Hatori [b], Katsuhide Igarashi [c], Ken-ich Aisaki [c], Jun Kanno [c], Yasuhiro Nakamura [a], Miwa Uzuki [d], Takashi Sawai [c], Hironobu Sasano [a,*]

[a] *Department of Pathology, Tohoku University Graduate School of Medicine, 2-1 Seiryo-machi, Aoba-ku, Sendai, Miyagi, 980-8575, Japan*
[b] *Department of Orthopedic Surgery, Tohoku University Graduate School of Medicine, Sendai, Japan*
[c] *Division of Toxicology, National Institute of Health Sciences, Biological Safety Research Center, Setagaya, Tokyo, Japan*
[d] *Department of Pathology, Iwate Medical College, Morioka, Japan*

Received 21 April 2006; revised 6 November 2006; accepted 14 November 2006
Available online 28 December 2006

Abstract

Effects of aromatase inhibitors (AIs) on the human skeletal system due to systemic estrogen depletion are becoming clinically important due to their increasing use as an adjuvant therapy in postmenopausal women with breast cancer. However, possible effects of AIs on human bone cells have remained largely unknown. We therefore studied effects of AIs including the steroidal AI, exemestane (EXE), and non-steroidal AIs, Aromatase Inhibitor I (AI-I) and aminoglutethimide (AGM), on a human osteoblast. We employed a human osteoblast cell line, hFOB, which maintains relatively physiological status of estrogen and androgen pathways of human osteoblasts, i.e., expression of aromatase, androgen receptor (AR), and estrogen receptor (ER) β. We also employed osteoblast-like cell lines, Saos-2 and MG-63 which expressed aromatase, AR, and ERα/β in order to further evaluate the mechanisms of effects of AIs on osteoblasts. There was a significant increment in the number of the cells following 72 h treatment with EXE in hFOB and Saos-2 but not in MG-63, in which the level of AR mRNA was lower than that in hFOB and Saos-2. Alkaline phosphatase activity was also increased by EXE treatment in hFOB and Saos-2. Pretreatment with the AR blocker, flutamide, partially inhibited the effect of EXE. AI-I exerted no effects on osteoblast cell proliferation and AGM diminished the number of the cells. hFOB converted androstenedione into E2 and testosterone (TST). Both EXE and AI-I decreased E2 level and increased TST level. In a microarray analysis, gene profile patterns following treatment with EXE demonstrated similar patterns as with DHT but not with E2 treatment. The genes induced by EXE treatment were related to cell proliferation, differentiation which includes genes encoding cytoskeleton proteins. We also examined the expression levels of these genes using quantitative RT-PCR in hFOB and Saos-2 treated with EXE and DHT and with/without flutamide. HOXD11 gene known as bone morphogenesis factor and osteoblast growth-related genes were induced by EXE treatment as well as DHT treatment in both hFOB and Saos-2. These results indicated that the steroidal aromatase inhibitor, EXE, stimulated hFOB cell proliferation via both AR dependent and independent pathways.

Keywords: Osteoblast; Aromatase inhibitor; Androgen; Estrogen; Exemestane

Introduction

Results in various epidemiological or clinical studies demonstrated that estrogens play important protective roles in human skeletal as well as cardiovascular systems, and estrogen deficiency resulted in accelerating the development of osteoporosis in postmenopausal women [1–3]. In breast cancer of postmenopausal women, hormone therapies without any clinically deleterious effects due to estrogen deficiency on bone metabolism as well as lipid metabolisms are preferable. Estrogen deficiency has been generally detected in the patients with breast cancer following chemotherapy induced ovarian failure, gonadotropin analogue, and aromatase inhibitors (AIs) therapy [4]. Aromatase is the pivotal enzyme of *in situ* or intratumoral estrogen biosynthesis in postmenopausal breast cancer patients, and catalyzes the conversion from androgens into estrogens (Fig. 1A). AIs therefore play an important role in

* Corresponding author. Fax: +81 22 273 5976.
E-mail address: hsasano@patholo2.med.tohoku.ac.jp (H. Sasano).

8756-3282/$ - see front matter © 2006 Elsevier Inc. All rights reserved.
doi:10.1016/j.bone.2006.11.029

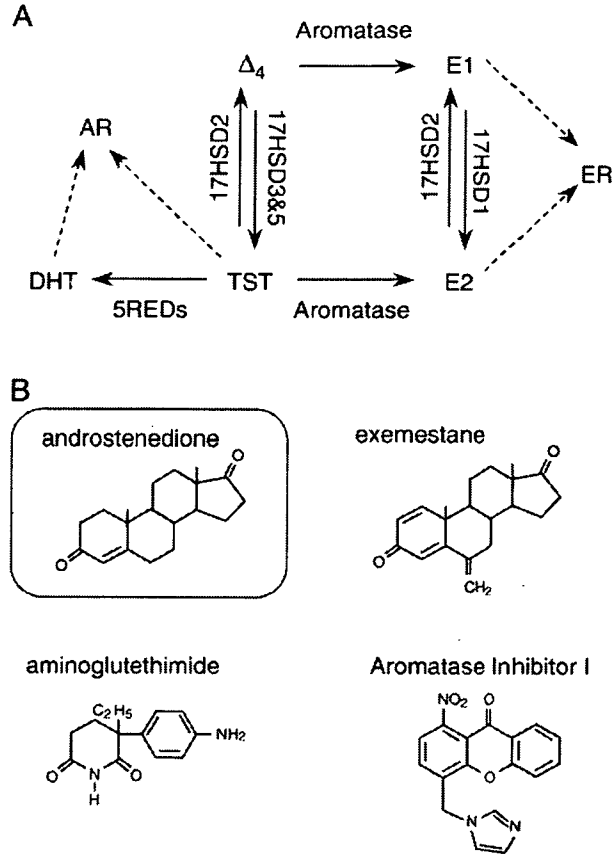

Fig. 1. (A) Summary of the pathway of estrogens and androgens production. Aromatase catalyzes the change from androstenedione (Δ4) and testosterone (TST) into estrone (E1) and estradiol (E2), respectively. 17HSD, 17β-hydroxysteroid dehydrogenase; 5REDs, 5α-reductase types 1 and 2; AR, androgen receptor; DHT, 5α-dihydrotestosterone; ER, estrogen receptor. (B) Structure of aromatase inhibitors used in this study. Androstenedione is a natural substrate of aromatase. Steroidal aromatase inhibitor, exemestane has an androstenedione-like structure.

clinical management of both primary and advanced breast cancer in postmenopausal women [5]. AIs are classified into two classes according to their modes of action. Type I AIs are steroidal inhibitions and one of them, exemestane (EXE) inhibits aromatase irreversibly and has an androstenedione (Δ_4)-like structure (Fig. 1B) [5–7]. Type II AIs are non-steroidal inhibitions and include aminoglutethimide (AGM), anastrozole, and letrozole [5].

Results of *in vivo* study using ovariectomized (OVX) rats demonstrated that EXE and its principal metabolite form, 17-hydroexemestane (17H-EXE) but not letrozole significantly prevented bone loss in OVX rats [8,9]. EXE and its principal metabolite, 17H-EXE, are structurally related to Δ_4 and bind to androgen receptor (AR) with relatively low affinity compared to 5α-dihydrotestosterone (DHT) [7]. These finding suggest that EXE may demonstrate protective effects toward bone tissues through its androgenic actions. However, detailed mechanisms of effects of EXE or androgen itself on human bone cells have remained largely unknown.

Various studies using human or animal bone tissues [10,11] and osteoblast cell culture using osteosarcoma cells [12,13] demonstrated that aromatase mRNA or protein was detected in osteoblast cells, which play an important role in bone remodeling. Therefore, in this study, we focused on effects of EXE in human osteoblast in an initial attempt to evaluate the effects of these AIs (summarized in Table 1 and Fig. 1B) [5–7,14], including AGM, EXE, and an experimental compound for inhibition of aromatase, Aromatase Inhibitor I (AI-I) [14] on human osteoblast and osteoblast-like cell lines. In our present study, we employed normal human cell line, hFOB, which maintains native characteristics of sex steroid hormone pathway of human osteoblasts, i.e., expression of AR, ERβ but not ERα, and aromatase. We also employed other osteoblast-like cell lines, Saos-2 and MG-63 which expressed ERα as well as ERβ in order to further study the mechanisms of effects of AI on human osteoblasts. We first examined the effects of estradiol (E2), DHT, progesterone (Prg), and AIs described above on cell proliferation of these cell lines, because the status of cell proliferation is important in the maintenance of homeostasis of bone tissue [15]. In addition, the effects of AIs on the conversion ratio of Δ_4 into E2 or testosterone (TST) in hFOB cultured medium were examined. We then screened E2, DHT, and EXE responsive genes using a microarray analysis in these cells, in order to further characterize the possible genomic effects of EXE on cell proliferation of osteoblasts. In this microarray analysis, hFOB was employed in order to examine the effects of E2, DHT, and EXE on native status of human osteoblasts but not on pathological status of osteoblasts such as osteosarcomas.

Materials and methods

Chemicals

Exemestane (EXE; FCE24304; 6-methyleneandrosta-1,4-diene-3,17-dione) and 17-hydroexemestane (17H-EXE; FCE25071; 6-methylenandrosta-1,4-diene-17β-ol-3-one) were obtained from Pfizer, Inc. (MI, USA). Aminoglutethimide (AGM) and Aromatase Inhibitor I [AI-I; 4-(Imidazolylmethyl)-1-nitro-9*H*-9-xanthenone] were obtained from Sigma-Aldrich Co. (MO, USA) and EMD Biosciences, Inc. (CA, USA), respectively. Estradiol (E2), progesterone (Prg), and RU38,486 (RU; mifepristone), spironolactone were obtained from Sigma-Aldrich. ICI 182,780 (ICI; fulvestrant) and hydroxyflutamide (OHF) were obtained from Tocris Cookson Inc. (MO, USA) and Toronto Research Chemicals, Inc. (Ontario, Canada), respectively. 5α-dihydrotestosterone (DHT) was obtained from Wako Pure Chemical industries, Ltd. (Osaka, Japan).

Table 1
Aromatase inhibitors used in this study

	Aminoglutethimide	Exemestane	Aromatase inhibitor I
Trademark [a]	Cytadren®	Aromasin®	–
Type [b]	Type II	Type I	Type II
Generation	First	Third	–
IC50 (nM) [c]	3000	50	40

[a] Cytadren® is trademark of Novartis Pharmaceutical Corporation. Aromasin® is trademark of Pfizer Inc. Aromatase Inhibitor I is non-clinical compound of Calbiochem®.

[b] Type I is steroidal compound. Type II is a non-steroidal compound.

[c] Refs, Aminoglutethimide and Exemestane are Miller et al. [5]; Aromatase Inhibitor I is Recanatini et al. [14].

These materials were dissolved in pure ethanol (Wako Pure Chemical industries) and serially diluted (final concentrations: 10^{-12} M to 10^{-5} M), respectively. AGM was dissolved in DMSO (Wako Pure Chemical industries). The final concentration of ethanol and DMSO used in this study did not exceed 0.05%.

Osteoblast cell and osteoblast-like cell lines and culture conditions

Human normal osteoblast cell, hFOB 1.19 cell line (CRL-11372) was obtained from American Type Culture Collection (VA, USA). hFOB 1.19 cell was cultured according to the protocol previously described [16]. The cell line was maintained in a mixture of Dulbecco's Modified Eagle Medium and Ham's F12 medium (1:1) without phenol red (Invitrogen Corporation, CA, USA) supplemented with 10% fetal bovine serum (FBS; JRH Biosciences, KS, USA) and 50 mg/mL G 418 sulfate (EMD Biosciences). Human osteosarcoma cell lines Saos-2 and MG-63 were provided from the Cell Resource Center for Biomedical Research, Tohoku University (Sendai, Japan) and were maintained in a RPMI-1640 (Sigma-Aldrich) with 10% FBS. These cells were pre-incubated for 24 h with FBS-free medium prior to examination in order to remove exo-/endogenous steroid hormones from the culture medium and study the effects of various compounds in the absence of steroids and also to synchronize the cell cycle. Different concentrations of test compounds were added, and the assay was terminated after 3 or 5 days by removing the medium from wells. Steroid blockers were added simultaneously.

Characteristics of hFOB, Saos-2, and MG-63

Expressions of relevant steroid receptors, i.e., ERα, ERβ, and AR were determined using quantitative RT-PCR methods in hFOB, Saos-2, and MG-63 cell lines. mRNA transcripts of steroid synthesis/metabolite enzymes, aromatase, 17β-hydroxysteroid dehydrogenase (17β-HSD) types 1, 2, 3, 4, and 5, and 5α-reductase (5α-Red) types 1 and 2 were all evaluated using RT-PCR methods. The details of quantitative RT-PCR including primer sets employed were previously described in detail [17,18]. Positive controls for these receptors and enzymes were cell lines of human breast cancer, T-47D, and human prostate cancer, LNCaP obtained from Cell Resource Center for Biomedical Research, Tohoku University (Sendai, Japan). Alkaline phosphatase (ALP), an osteoblast-specific marker, was also studied using RT-PCR for characterization of these cell lines.

Estradiol and testosterone production assay

hFOB cells were plated in 10 mm dishes at a density of 10^6 viable cells and cultured for 48 h. Then media were changed to FBS-free medium, and hFOB cells were incubated with 10^{-7} M androstenedione (Δ_4; Sigma-Aldrich) in the presence or absence of EXE or AI-I (10^{-7} M). The media were then collected after 24 h, and E2 and TST were measured by solid-phase radioimmunoassay. Radioimmunoassay was performed in SRL Inc. (Tokyo, Japan) using DPC estradiol kit and DPC total testosterone kit (Diagnostic Products Corporation, LA, USA). In addition, we confirmed that the concentrations of E2 and TST were under the detection limits (E2, 5 pg/mL; TST, 30 pg/mL) in the serum- and phenol red-free medium.

Cell proliferation assay

hFOB, Saos-2, and MG-63 cells were treated with steroids and test compounds for 24, 48, and 72 h, when specimens were harvested and evaluated for cell proliferation using the WST-8 method (Cell Counting Kit-8; Dojindo Inc., Kumamoto, Japan) [18]. Optical densities (OD, 450 nm) were evaluated using a SpectraMax 190 microplate reader (Molecular Devices, Corp., CA, USA) and Softmax Pro 4.3 microplate analysis software (Molecular Devices). The status of proliferation (%) was calculated according to the following equation: (cell OD value after test materials treated/vehicle control cell OD value) × 100.

Alkaline phosphatase activity assay

hFOB, Saos-2, and MG-63 cells were plated in 48 well plate at a density of 10^6 viable cells and cultured for 48 h. All cell lines were treated with 10^{-9} to 10^{-7} M exemestane for 72 h, when cells were lysed with 0.05% Triton X-100 (Wako Pure Chemical industries) and evaluated for alkaline phosphatase activity

Table 2
Primer sequences used in quantitative RT-PCR analysis

cDNA	GB#	Sequence	cDNA position	Size (bp)
MYBL2	NM_002466	Forward 5′-GTAACAGCCTCACGCCCAAGA-3′ Reverse 5′-TCCAATGTGTCCTGTTTGTTCCA-3′	1522–1615	94
OSTM1	NM_014028	Forward 5′-TTGAGAATAAGGCTGAACCTGGAAC-3′ Reverse 5′-TTACAGGCACTGTGTCACTGCAAG-3′	801–926	126
HOXD11[a]	NM_021192	Forward 5′-CAC TGT CCT TGG GTT TAA TG-3′ Reverse 5′-GGT AAA ATT GTA ACG GGA CG-3′	1091–1245	174
GPC2	NM_152742	Forward 5′-AGA AAT GTG GTC AGC GAA GC-3′ Reverse 5′-ACA CCT TCG CAC TGT TTT CC-3′	871-1183	313
ADCYAP1R1	NM_001118	Forward 5′-CAG CAA AAG GGA AAG ACT CG-3′ Reverse 5′-GAG CTG CTC TTG CTC AGG AT-3′	1351–1584	234
COL1A1	NM_000088	Forward 5′-GGT GGT GGT TAT GAC TTT GGT T-3′ Reverse 5′-CTT GGC TGG GAT GTT TTC AGG T-3′	3784–4092	309
SMAD1[a]	NM_005900	Forward 5′-GGT TCA CCT CAT AAT CCT-3′ Reverse 5′-CCT TTG TCA GTT CTC AAT C-3′	1779–1887	127
SMAD5[a]	NM_005903	Forward 5′-AGC TAA AGC CGT TGG ATA-3′ Reverse 5′-AGG CAC TAA TAC TGG AGG T-3′	668–768	119
RUNX2	NM_004348	Forward 5′-GTG GAC GAG GCA AGA GTT T-3′ Reverse 5′-TAC TGG GAT GAG GAA TGC G-3′	782–961	198
SPARC	NM_003118	Forward 5′-CCT GTA CAC TGG CAG TTC-3′ Reverse 5′-CCA GGG CGA TGT ACT TGT C-3′	793–937	163
ALP	NM_000478	Forward 5′-ACC ATT CCC ACG TCT TCA CA-3′ Reverse 5′-AGA CAT TCT CTC GTT CAC CGC C-3′	1379–1540	162
RPL13A	NM_012423	Forward 5′-CCT GGA GGA GAA GAG GAA AGA GA-3′ Reverse 5′-TTG AGG ACC TCT GTG TAT TTG TCA A-3′	487–612	126

GB#, GeneBank accession number.
All primer sets were designed using OLIGO Primer Analysis Software (TAKARA Bio Inc., Shiga, Japan).
[a] Forward and reverse primers were located in sama exon.

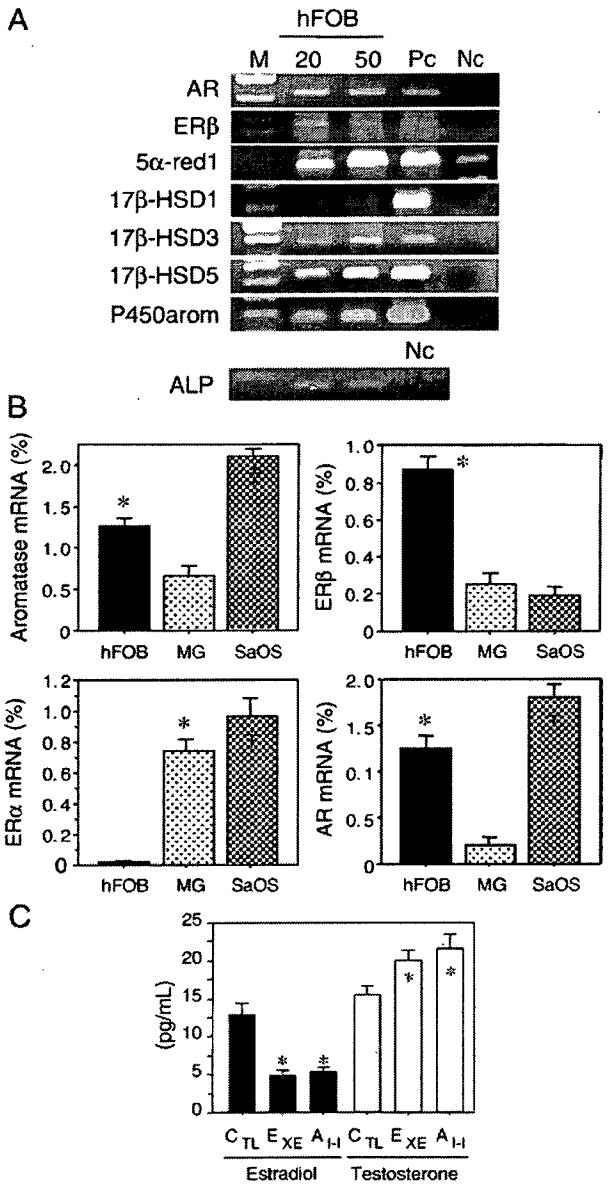

Fig. 2. (A) Results of RT-PCR analysis of steroid hormone receptors and steroid-related enzymes. Both 20 and 50 ng/μL cDNA of hFOB were used for PCR (ALP was 20 ng/μL alone). AR, androgen receptor; ER, estrogen receptor; 5α-red1, 5α-reductase type 1; 17β-HSD, 17β-hydroxysteroid dehydrogenase; P450 arom, aromatase; M, molecular marker; Pc, positive control; Nc, negative control. (B) Expression levels of aromatase, AR, ERα, and ERβ in hFOB, Saos-2, and MG-63. $*p<0.05$ vs. MG-63 (aromatase and AR), vs. MG-63 and vs. Saos-2 (ERβ), vs. hFOB (ERα); $^{\dagger}p<0.05$ vs. hFOB and MG-63 (aromatase and AR), vs. MG-63 and hFOB (ERα). (C) Estradiol and testosterone productions in hFOB cells. The data are expressed as the mean SD ($n=3$). $*p<0.05$ vs. control cells (CTL). EXE, 10^{-7} M exemestane; AI-I, 10^{-7} M aromatase inhibitor I.

using the *p*-nitrophenylphosphate method (LabAssay ALP; Wako Pure Chemical industries) [19]. Optical densities (OD, 405 nm) were evaluated using a SpectraMax 190 microplate reader (Molecular Devices) and Softmax Pro 4.3 microplate analysis software (Molecular Devices). ALP activity (units/μL)=(concentration of *p*-nitrophenol/15 min)×1 (dilution factor of sample). The ALP activities were presented as units/μL/10^6 cells. The ALP activity levels in each case were represented as a ratio of vehicle control (%).

Microarray analysis

The procedure was based on a previously reported study [20]. Cell lysates were prepared using RLT buffer (QIAGEN GmbH, Hilden, Germany). Total RNA was extracted using RNeasy Mini Kit (QIAGEN). First-strand cDNA was synthesized by incubating 5 μg of total RNA with 200 U SuperScript II reverse transcriptase (Invitrogen), 100 pmol T7-(dT)24 primer (Invitrogen). Ten units of T4 DNA polymerase (Invitrogen) were then added, and the dsDNA was mixed with T7 RNA polymerase (Invitrogen). The purified cRNA was fragmented at 300–500 bp as target solution. Hybridization was performed with the GeneChip Human Genome 133 ver. 2.0 (Affymetrix, Inc., CA, USA). The reacted arrays were then scanned as digital image files and scanned data were analyzed with GeneChip software (Affymetrix). Relative levels of gene expression were calculated by global normalization.

Data were subjected to hierarchical clustering analysis and visualization using the Cluster and TreeView programs (Stanford University) in order to generate tree structures based on the degree of similarity, as well as matrices comparing the levels of expression of individual genes in each sample [21].

Real-time PCR

Real-time PCR was carried out using the LightCycler System and the FastStart DNA Master SYBR Green I (Roche Diagnostics GmbH, Mannheim, Germany). The primer sequences used in this study are summarized in Table 2. An initial denaturing step of 95 °C for 10 min was followed by 35 cycles, respectively, at 95 °C for 10 min; 15 s annealing at 65 °C (ALP, COL1A1), 64 °C (MYBL2, OSTM1, RPL13A), 62 °C (SMAD1, SMAD5, SPARC, RUNX2), or 60 °C (HOXD11); and extension for 15 s at 72 °C. Negative control experiments included those lacking cDNA substrates to confirm the presence of exogenous contaminant DNA. No amplified products were detected under these conditions. The mRNA levels in each case were represented as a ratio of RPL13A (%) [22].

Immunohistochemistry of AR

Five non-pathological bone tissues were retrieved from surgical pathology files (two females and three males, 17 to 55 years old) of Department of Pathology, Tohoku University Hospital (Sendai, Japan).

Tissue sections were immunostained using a biotin-streptavidin method with Histofine kit (Nichirei Co. Ltd., Tokyo, Japan). The monoclonal antibody for AR (AR411) [23] was obtained from DakoCytomation (Kyoto, Japan). Experimental procedures employed in our present study have been previously described in detail [22,23]. The dilutions of primary AR antibody were 1:100. The antigen-antibody complex was then visualized with 3,3′-diaminobenzidine solution, and counterstained with hematoxylin. Prostate cancer was used as a positive control for AR. Normal mouse IgG was used as a negative control for immunostaining and no specific immunoreactivity was detected.

Statistical analysis

Results were expressed as mean±SD. Statistical analysis was performed with the StatView 5.0 J software (SAS Institute Inc., NC, USA). All data were analyzed by analysis of variance (ANOVA) followed by post hoc Bonferroni/Dunnett multiple comparison test. A p-value <0.05 was considered to indicate statistical significance.

Results

Characteristics of hFOB, MG-63, and Saos-2 cell line

Characteristics of osteoblast and osteoblast-like cell lines are summarized in Figs. 2A and B. hFOB cells expressed mRNA transcripts of AR and ERβ. Relatively low level of ERα mRNA transcript was detected in hFOB cells. Aromatase, 17β-HSD type 1, 3, and 5, and 5α-Red types 1 and 2 mRNA transcripts were all detected in hFOB cells by